Research article

Thermal self-crosslink after etching for regulated preparation of Ti$_3$C$_2$ type MXene membrane and its preliminary gas separation

Nong Xu [a,b,1], Chen Pan [a,1], Shenzhen Qu [a], Qiao Liu [a,b], Qing Wang [a], Qiang Dong [a,*], Long Fan [a,**]

[a] *School of Energy, Materials and Chemical Engineering, Hefei University, Hefei, 230601, China*
[b] *State Key Laboratory of Biochemical Engineering, Institute of Process Engineering, Chinese Academy of Science, Beijing, 100190, China*

ARTICLE INFO

ABSTRACT

We present an innovative methodology for the synthesis of MXene membranes through a dual-stage process involving etching and subsequent thermal self-crosslinking. A molar ratio of 1 (Al^{3+}):9 (F^-) using HCl/LiF was employed to convert raw Ti$_3$AlC$_2$ (MAX phase) into MXene within 48 h at 40 °C. This procedure predominantly yielded monolayers distinguished by diameters exceeding 500 nm, elevated crystallinity and a high overall yield. Advanced characterization techniques, including FESEM, TEM, HRTEM, AFM, XPS, and FTIR, were utilized. Instrumental analysis confirmed the formation of MXene exhibiting a single-flake morphology with diameters exceeding 500 nm. These monolayers were intact and continuous, with smooth peripheries and a uniform thickness of 2.1 nm. The surfaces were predominantly composed of carbon (C), oxygen (O), and titanium (Ti) atoms, interconnected by chemical bonds such as C–Ti–O, C–Ti–OH, C–C, C–O, and Ti–O. In the subsequent phase, vacuum filtration facilitated the assembly of a self-supporting MXene membrane. Thermal treatment at 170 °C for 30 h resulted in the reinforcement of C–Ti–O bonds within the nanosheets, increasing their prevalence to 43.14 % and 19.47 %, respectively. This thermal regulation reduced the interlayer *d*-spacing from 4.33 to 3.54 Å, which significantly improved the gas separation efficiency beyond the Knudsen diffusion limit, as demonstrated by the α_{H_2/CF_4} value exceeding 23.0.

1. Introduction

Two-dimensional materials are defined by their single or few-atom-thick layers, which confer unique physical, chemical, and mechanical properties [1,2]. MXene, a class of two-dimensional (2D) materials, has emerged as a subject of intense research interest due to its exceptional properties and potential applications. MXenes stand out for their high electrical conductivity, hydrophilicity, mechanical flexibility, and thermal stability. These properties make MXene family highly suitable for a range of applications, from energy storage devices like batteries and supercapacitors to electromagnetic interference shielding, sensor technology, and even biomedical applications [3–6]. MXene is derived from a larger class of compounds known as MAX phases, which are ternary carbides or nitrides. The general formula for MXene is M$_{n+1}$X$_n$T$_x$, where M represents a transition metal, X is carbon and/or nitrogen, and T$_x$

---

* Corresponding author.
** Corresponding author.
  E-mail addresses: qdong@hfuu.edu.cn (Q. Dong), fanlong@hfuu.edu.cn (L. Fan).
[1] The two authors contributed equally to this work.

denotes surface terminations such as –OH, –O or –F. In many MAX phases, the metallic bonds between M and A layer atoms are weaker than the ionic or covalent bonds between M and X atoms. Therefore, an etchant can be introduced to break the metallic bonds between M and A layer atoms, thereby achieving the purpose of MXene nanosheet delamination [7–9]. The discovery of MXene can be traced back to 2011 when researchers at Drexel University developed a novel etching process to selectively remove the A layer from the MAX phase. This process resulted in the exfoliation of the material into 2D layers, thus creating MXene. The initial discovery has since sparked a surge in research aimed at understanding and harnessing the properties of MXenes [10,11].

Over the years, the preparation techniques for MXene have significantly improved. Researchers have focused on refining the etching process to enhance the quality and yield of MXene. This has involved the development of less harsh etching conditions, the exploration of different etchants, and the optimization of intercalation methods to separate the MXene layers gently [12]. Wet chemical etching is one of the most mature technologies for the synthesis of MXene nanosheets. Typical MXene is generated by selective etching of layered ceramic Ti_3AlC_2 (MAX) [13,14]. Different concentrations of HF are introduced to etch Ti_3AlC_2 containing aluminum (Al) atoms. Although HF has been proven to be a very good etchant for removing Al, it is highly corrosive, thus posing serious safety risks. This should be paid extra attention to during the preparation process of MXene. Fluoride salts, such as LiF, NaF, KF, etc., when mixed with hydrochloric acid (HCl) or other acids for etching precursor like Ti_3AlC_2, represent another safer preparation method. Hydrochloric acid and metal fluorides will form HF and intercalation ions [15,16]. For example, if LiF is used, the intercalation ion would be Li^+. Therefore, the advantage of this method is that the etching, intercalation, and delamination steps can be carried out simultaneously. Although this method is only applicable to a few MXenes, the $Ti_3C_2T_X$ flakes produced by it can reach lateral dimensions of up to 15 mm and are pinhole-free [17]. Moreover, by using LiCl to replace organic molecules for interlayer insertion, the yield of single-layer MXene nanosheets can be increased to 60 %, or even higher. Generally, the in-situ chemical etching has taken advantageous of higher production, safer procedures, and easier handling [18]. we follow the process of the method and systematically investigate three different etchants, the etching ratios and the MXene nanosheets thus produced.

The unique properties of MXene align with the technological needs of human research for the next generation of separation and purification. So far, MXene has been used in a wide range of studies on membrane materials/technologies for separation/purification. MXene nanosheets are used to prepare membrane with separation performance by vacuum self-assembly, in which filtration is the most prevalent method. After vacuum filtration, the layered 2D nanosheets has regular and controllable nanoscale transport channels, which can achieve the transport of liquid/gas molecules and effectively screen molecules of different sizes. For wastewater treatment, for example, Ding and others [19] obtained $Ti_3C_2T_X$ membrane through vacuum filtration. MXene nanosheets, ranging in size from 100 to 400 nm, were employed to construct layered channels that facilitate the transport of water molecules. Subsequently, positively charged $Fe(OH)_3$ nanoparticles were introduced between the MXene layers. This insertion maintained an expanded interlayer spacing, enhancing the overall structure for efficient molecular separation. This combined strategy achieved a water flux in the MXene membrane that far exceeds 1000 L m^{-2} h^{-1} bar^{-1}. Although still in the initial stages, MXene has already shown great potential in membrane-based gas separation. Ding et al. [20] prepared MXene membrane through vacuum-assisted filtration on an Anodic Aluminum Oxide (AAO) substrate. Gas permeation tests conducted at 25 °C and 1 bar showed that the membrane has a high degree of permeability to small molecule gases, such as He and H_2. Shen and his colleagues [21] utilized MXene nanosheets with borate ($B_4O_7^{2-}$) and Polyethyleneimine (PEI) to create cross-linking, where the borate/PEI intercalates between the layers of MXene. This membrane can be used to separate CO_2 and CH_4 (or N_2), and the cross-linking also enhances the mechanical strength of the MXene membrane. Moreover, compared to the original pure MXene membrane, the borate/PEI intercalated MXene membrane increased the CO_2 adsorption capacity by 43 %. In addition to room temperature operation, MXene membranes can also be used for the separation of gases with small kinetic diameters at high temperatures. The research results of Fan et al. [22] indicate that MXene membranes have a selectivity of up to 41 for H_2/N_2 separation at 320 °C.

The transport channel of MXene membrane is formed by the pinholes, internal spacings between parallel and wrinkled nanosheets known as nanogalleries, and voids between the nanosheet edges which can be considered as nanoslits [23]. Therefore, factors such as thickness, lateral size and interlayer distance of MXene nanosheet have a decisive influence on the membrane properties. These factors usually are co-decided by the synthesis of MXene nanosheets and preparation of MXene membrane. During the preparation, the weak interlayer interaction leads to unstable structure of MXene membrane, and the molecular sieve channel is easily destroyed, resulting in loss of separation ability. Therefore, it is particularly important to establish strong interlayer force between MXene layers and prepare the membrane with stable structure and molecular sieve channels. Several strategies have been studied to solve such problems, such as epoxy resin encapsulation [24], small molecule covalent cross-linking [25,26], and thermal self-crosslinking [27]. Thermal self-crosslinking is a post-synthesis treatment that enhances the structural integrity and stability of MXene membrane. By heating the MXene films to specific temperatures, typically above 100 °C, crosslinks form between the layers, reducing the interlayer spacing and improving mechanical strength. This process is vital for gas separation applications, where membranes must exhibit selective permeability and durability.

The highlight of this study is thermal self-crosslinking between layers after the etching. The thermal regulating method, which is facile, convenient and flexible to operate, is used to regulate the distance and interlayer force between the nanosheets, thereby initially achieving gas separation. Our advancements have led to the development of MXene membranes with finely tuned separation properties. These membranes show promise for hydrogen separation in industrial applications.

2. Experimental

2.1. Materials

Titanium aluminum carbide (Ti_3AlC_2, 400 mesh, 80 %) was purchased from Nanjing Xianfeng Nano Material Technology Co., Ltd. Hydrochloric acid (HCl, AR, 36–38 %) was bought from Wuxi Prospect Chemical Reagent Co., Ltd. Lithium fluoride (LiF, AR, 99 %), Hydrofluoric acid (HF, AR, 50 %), and Ammonium bifluoride (NH_4HF_2, AR, 98 %) were purchased from Shanghai Titan Technology Co., Ltd. Deionized water (DI water, ER = 18.5 MΩ cm^{-1}) was prepared in the laboratory. All the chemicals and reagents employed in this work were used directly without further purification.

### 2.2. Preparation of single-layer MXene

2 g of Ti_3AlC_2 was added to HCl/LiF mixed solution with stirring at 40 °C in a 50 mL Teflon beaker for 48 h. Then, washed by DI water and centrifuged at 3500–9000 rpm. When pH reached neutral, dispersing the collected sedimentation in DI water using ultrasonication (input power 150 W, frequency 40 kHz) for 1.5 h in an ultrasonic container (Model: KQ3200DE, Kunshan Ultrasonic Instrument Co., Ltd. China) with an ice-water mixture at a theoretical temperature of 0 °C. The obtained suspension was centrifuged again for collecting single (and/or few) layer MXene nanosheets at 3500 rpm for 1h. The used acid was poured into a special waste collection bucket and handed over to the Hefei Environmental Protection Company for harmless neutralization treatment. For HF and NH_4HF_2, simply replace the HCl/LiF and repeat the whole procedure.

2.3. Preparation of MXene membrane and its gas separation

Self-assembly MXene membrane was prepared on an aqueous MCE (mixed cellulose) microporous substrate (0.1 μm, Haiyan New Oriental Plasticization Technology Co., Ltd., China) with vacuum-assisted filtration. The diagrammatic sketch was shown in Fig. 1(a) and (b). After drying at room temperature in Fig. 1(c), the MXene membrane naturally peeled off the substrate. Fig. 1(d) and (e) showed the flexibility and actual size of the MXene membrane prepared with the vacuum-assisted self-assembly method.

The MXene membrane was vacuum-dried at 25 °C for 24 h, and placed in a vacuum oven and heat treated 30 h at 25 °C, 80 °C, 110 °C, 140 °C and 170 °C, respectively. After cooling down, the membrane was moved to gas measurement rig as shown in Fig. 2.

All gas permeation measurements were conducted by a homemade membrane module as shown in Fig. 2. A pair of silicone gaskets and a 0.1 μm Nylon-66 disc were employed as soft gaskets and supporting-substrate to avoid the leakage between the stainless-steel module (shown in Figure S1 in the Supplemental information) and the MXene membrane. The gas transport through the MXene membrane was measured using the constant pressure, variable volume method. The permeability was calculated from Eq. (1),
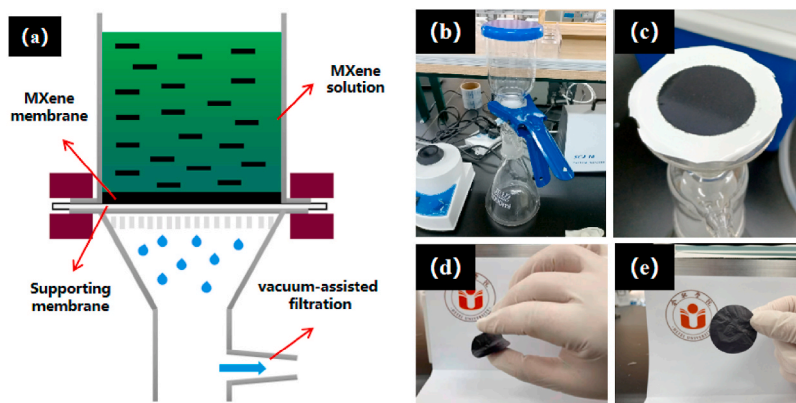
(a) Schematic diagram of the vacuum-assisted filtration of MXene nanosheets,

(b) Picture of glass filtration device,

(c) the self-assembly MXene membrane (central black disc),

(d) Supportless self-assembly MXene membrane remains intact after rolling and

folding, and (c) Self-assembly MXene membrane with the Hefei university logo

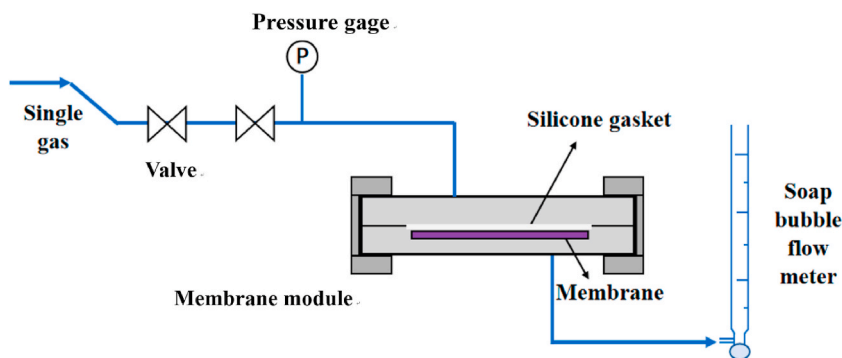**Fig. 1.** Preparation of the vacuum-assisted self-assembly MXene membrane.

Fig. 2. Schematic diagram of gas permeation testing rig.

$$P_i = V_i/4.032 \times A \times \Delta P_i \tag{1}$$

where P_i is the gas i permeation rate, Gas permeation unit (GPU), V_i represents the rate at which the gas i passes through the membrane, ml·min^{-1}, A is the test film area, m^2, ΔP_i is the pressure difference between the gas i on both sides of the membrane, kPa.

The ideal selectivity of two components was calculated as Eq. (2):

$$\alpha = P_i/P_j \tag{2}$$

where α is the ideal selectivity, P_i and P_j are the permeability of each component, GPU. The gas permeability and selectivity were calculated by Eqs. (1) and (2).

2.4. Characterization and measurement

XRD analysis was conducted by Dandong Tongda TD-3500 (China) with filtered Cu−Kα radiation (30 kV and 20 mA, λ = 1.54 Å), where the step was 0.02° and the step time was 1 s. The well-known Bragg's law (Eq. (3)) was used to calculate the interlayer distance (*d*-distance) of MXene nanosheets.

$$d = n\lambda/sin\,\theta \tag{3}$$

here *d*: crystal plane distance, nm, *θ*: diffraction half-angle, *λ* is the wavelength of X-rays, take λ = 0.15406 nm, *n* is the diffraction series, take the first level of diffraction.

Field Emission Surface Scanning Electron Microscope (FESEM) (SU8010, Hitachi, Japan) was used to scan the MXene with different amounts to explore their surface morphologies on the AAO substrate. Some samples were treated by gold-spraying (SuPro Instruments LTD, ISC 150) for good electrical conductivity before the FESEM observation. Transmission Electron Microscope (TEM) (JEM-F200, Japan JEOL) was employed to characterize MXene nanosheets. High-Resolution Transmission Electron Microscopy (HRTEM) (FEI Tecnai G2F20, 200 KV, USA) images were obtained to verify their micro-morphologies and structures, especially the structure of a few atomic layers. Surface topographies and three-dimensional (3D) images were obtained by Atomic Force Microscopy (AFM, Bruker Dimension Edge, USA) with 3 μm × 3 μm scan area. Surface microstructure and functional groups of the MXene membrane were observed with a fourier transform infrared spectrometer (FTIR) (Nicolet iS 50+ Contiuum, Thermo Fisher, USA). The range of the wavelength was from 400 to 4000 cm^{-1}. The variation of chemical structure was discussed based on the FTIR scanning. X-ray photoelectron spectroscopy (XPS) (ESCALAB™ 250Xi, Thermo-Fisher Scientific Instrument, USA) was employed to qualitatively analyze the surficial chemical structure of the MXene and MXene membrane. The size distribution of MXene nanosheets was detected by Malvern Zetasizer Nano ZS90 (UK) with the dispersion solvent of DI water.

Table 1
Different etchants and the same ratio of Al^{3+}: F$^-$ (Ti$_3$AlC$_2$: HF).

Ti$_3$AlC$_2$	HF (50 wt%)	NH$_4$HF$_2$	HCl (36 wt%)	LiF	Ratio of Al^{3+}:F$^-$	Product name
2.0 g	2.88 ml	–	–	–	1:7	HF-MXene
2.0 g	–	2.05 g	–	–	1:7	NH4-MXene
2.0 g	–	–	28 ml	1.87 g	1:7	Li-MXene

3. Results and discussion

3.1. Effects of three etchants

Ti$_3$AlC$_2$ is the most widely studied MAX phase and a variety of etchants have been developed for the Ti$_3$AlC$_2$ [28–30]. In this work, HF, NH$_4$HF$_2$ and HCl/LiF were selected as etchants as shown in Table 1. The volumes and dosages of different acids were also listed in Table 1.

Molar ratio of Al^{3+} to F$^-$ ions for each reaction was 1:7. The productions were named HF-MXene, NH$_4$-MXene, and Li-MXene, respectively. Upon comparing Fig. 3(g) and (h), and 3(i) with Fig. 3(a), (b), and 3(c), as well as Fig. 3(d), (e), and 3(f), it is evident that the Li-MXene nanosheets display a pronounced stratification, with layers stacked upon one another. In contrast, the HF-MXene and NH$_4$-MXene samples are characterized by multilayered particles that suggest partial etching, indicative of an incomplete delamination process. Fig. 3(j) shows four different XRD patterns from top to bottom, labeled as HF-MXene, Li-MXene, NH$_4$-MXene and PDF #52–0875. The bottom pattern is the standard Powder Diffraction File (PDF) for diffraction data of Ti$_3$AlC$_2$.

As illustrated in Fig. 3(j), each of the as-synthesized MXene exhibits a diffraction pattern that deviates from the standard PDF. The characteristic peak of the Al at 39° disappear after etching, while the locations of (002) peaks all move down to lower angles. This
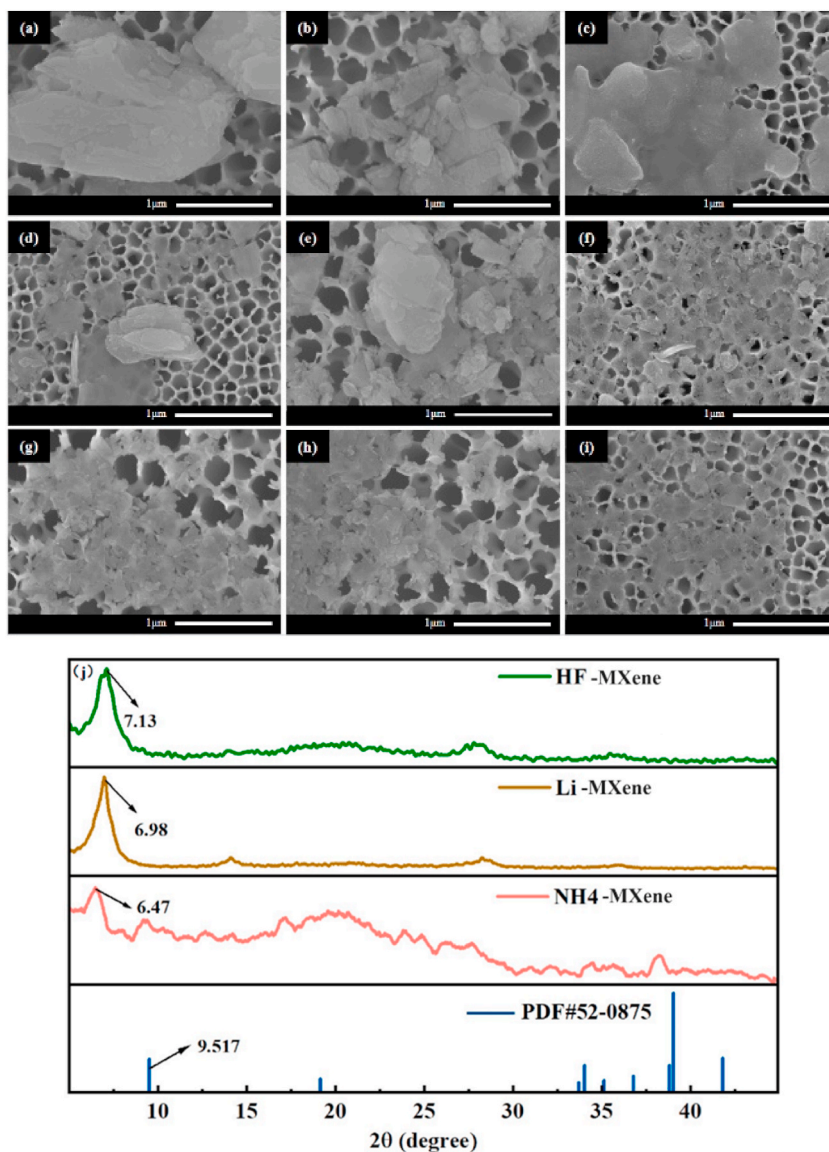

Fig. 3. 48 h etching with (a), (b), (c) HF, (d), (e), (f) NH$_4$HF$_2$ and (g), (h), (i) HCl/LiF, respectively, (j) XRD of HF-MXene, Li-MXene, NH$_4$-MXene and Ti$_3$AlC$_2$.

phenomenon means that different types of acids have corroded Ti_3AlC_2 to varying degrees, thereby altering its original structure and the corresponding XRD patterns. According to the Bragg Equation, the *d*-spacings of HF-MXene, NH$_4$-MXene and Li-MXene are 1.24, 1.37 and 1.27 nm, respectively. The larger *d*-spacing of NH4-MXene or Li-MXene can owe to NH_4^+ or Li^+ embedded between MXene nanosheet layers during etching. Additionally, the Full Width at Half Maximum (FWHM) for the (002) peak is 1.054° for HF-MXene, 1.338° for NH$_4$-MXene, and 0.734° for Li-MXene. Apparently, the Li-MXene is smaller than the other two, which indicated that Li-MXene has a higher degree of crystallinity.

3.2. Al^{3+} and F^- molar ratios

The product Li-MXene, obtained by etching the Ti_3AlC_2 with HCl/LiF, exhibits a larger *d*-spacing and a higher degree of crystallinity. Therefore, it is important to further investigate the impact of the molar ratios of Al^{3+} and F^- on the formation of MXene nanosheets. HCl/LiF, with the molar ratios of 1:3, 1:5, 1:7, 1:9, is listed in Table 2. The corresponding products were named F3, F5, F7, and F9, respectively.

Fig. 4(a)–4(d) respectively show the SEM images of F3 to F9, while Fig. 4(e)–4(h) correspond to the magnified photographs of F3 to F9. The SEM images of F7 and F9 show that the nanosheets have uniform size, smooth surface, and similar transparency. Moreover, the AAO substrate can be clearly seen under the sample sheets, indicating the nanosheets have uniform thickness and single-layer structure.

As the concentration of F^- increased from F3 to F9, the (002) peak of MXene shift from 6.894° to 6.161° in Fig. 4(j). This is attributed to the insertion of more Li^+ ions between the MXene layers, which expand the *d*-spacing. In Fig. 4(j), ratios of 1:7 and 1:9 can further enlarge the *d*-spacing, thereby making it easier to obtain the etching effect of single-layer sheets. Additionally, under the same molar ratio of 1:9, acids HF, HCl/LiF and NH$_4$HF$_2$, were used to etch Ti_3AlC_2, respectively. The results from Fig. 4(k) show that the particle size distribution of Li-MXene is relatively larger. Therefore, the ratio of 1:9 was selected to synthesize predominantly single-layer nanosheets with a larger size.

3.3. Characterization of the prepared MXene

Through a series of experiments in the above two sections, using the HCl/LiF and the precursor Ti_3AlC_2 (MAX) specified in the fifth row of Table 2, MXene products with a larger average area, uniform thickness, and single-layer flake appearance were prepared under the condition of the molar ratio of Al^{3+} to F^- being 1:9. Subsequently, we carried out instrumental characterization and measurement of the corresponding MXene. Fig. 5 has two FESEM images. Fig. 5(a) displays a large block of the MAX phase precursor Ti_3AlC_2, which is a typical three-dimensional cubical structure. Fig. 5(b) clearly shows the complete overview of a two-dimensional MXene nanosheet, with its edges appearing irregularly shaped. The dimensions of the nanosheet structure extend to approximately, or exceed, 500 nm both in width and height. Through the MXene nanosheet, the pores on the surface of the AAO substrate underneath can be discerned quite clearly, indicating that the MXene prepared in this study is extremely thin nanosheets.

The sample's microstructure and the fine structure were determined through TEM and HRTEM. Fig. 6(a) shows a large single MXene flake with a diameter exceeding 1 μm. Fig. 6(b) is a magnified view of Fig. 6(a), from which it can be seen that the edges of the single MXene flake are smooth and easily bent. Additionally, Fig. 6(c) under HRTEM observation shows the overlapped image of two MXene nanosheets. The single flake in Fig. 6(a) and the stacking in Fig. 6(c) can be cross-verified with Fig. 5(b). They all indicate that the extremely thin layering and the structure of sheets stacked layer by layer may create countless channels between the layers, which facilitates the permeation and separation of gas molecules. Fig. 6(d) is an HRTEM image of MXene, and the measured lattice spacing is 0.276 nm, the same as the interlayer spacing of the MXene (100) facet, proving the existence of the MXene phase. Furthermore, the single-crystal region of MXene can be clearly identified, displaying regularly oriented lattice stripes, further revealing that the sample is composed of Ti_3C_2 type MXene.

Fig. 7 shows the results of MXene measurement by AFM within a 3 μm by 3 μm area. The AFM detection further confirmed the two-dimensional surface and micro-morphology of the MXene single flake, as well as the flatness and continuity of the single flake. The thickness of the MXene nanosheet layer was measured at four different positions in Fig. 7, labeled (a), (b), (c), and (d). The height variation curves of the AFM probe movement are shown in Fig. 7(a), (b), 7(c) and 7(d), respectively, with thicknesses of 2.0, 2.1, 2.2, and 2.1 nm. Based on the measurement, it can be known that the average thickness of a single-layer MXene is about 2.1 nm.

The XPS spectrum of Fig. 8(a) shows the untreated MXene mainly contains four elements: C, O, Ti and F. After comparison with the literature [20,31–36], we have deconvoluted the peaks of C1s, O1s, Ti2p and F1s. Fig. 8(b) displays the C1s of MXene, where the peak at 281.9 eV can be attributed to C–Ti, the peak at 284.9 eV can be attributed to C–C. It is possibly due to the selective dissolution of Ti during the etching process, leading to the formation of C–C bonds. Fig. 8(c) shows the O1s of MXene, where the peaks at 529.7 eV and

Table 2
Different molar ratios of Al^{3+}: F^- (Ti_3AlC_2: HF).

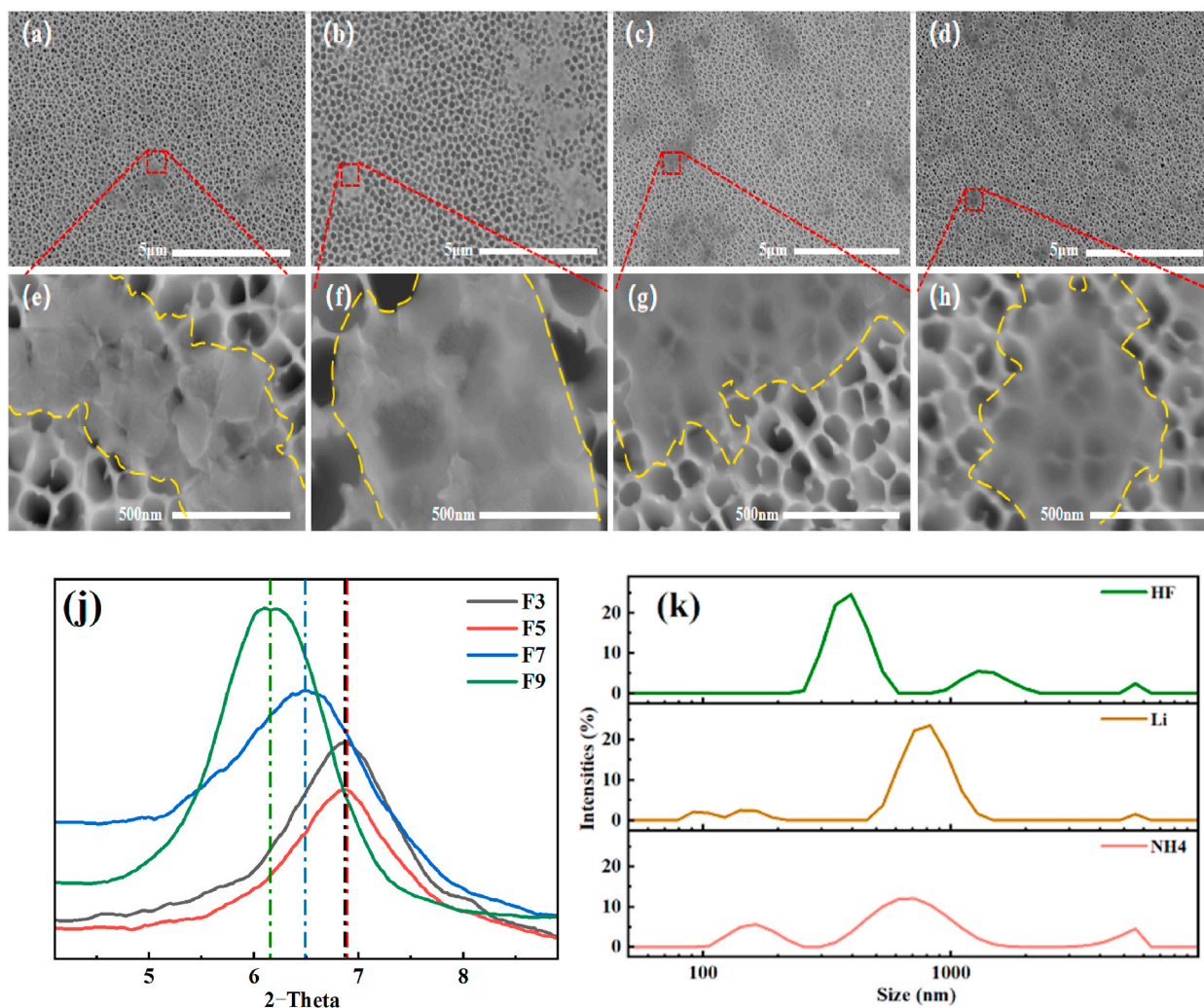| Ti_3AlC_2	HCl (36 wt%)	LiF	Ratio of Al^{3+}:F^-	Sample name
2.0 g	12 ml	1.07 g	1:3	F3
2.0 g	20 ml	1.33 g	1:5	F5
2.0 g	28 ml	1.87 g	1:7	F7
2.0 g	36 ml	2.40 g	1:9	F9

Fig. 4. SEM of (a), (e) F3, (b), (f) F5, (c), (j) F7 and (d), (h) F9, (j) XRD of F3, F5, F7 and F9, (k) Size distributions of HF-MXene, Li-MXene, NH4-MXene with each molar ratio 1:9.
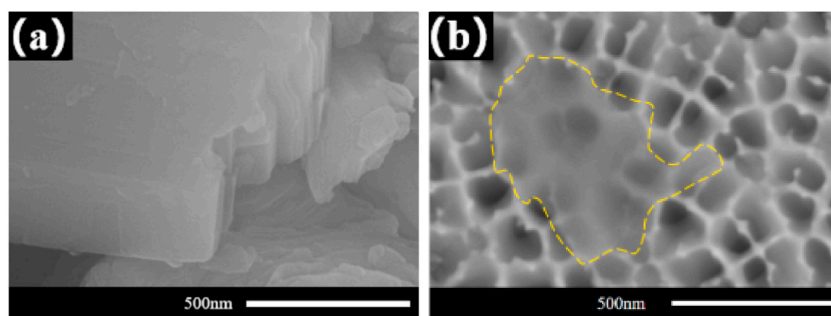

Fig. 5. FESEM of sample F9 in Table 2 (a) the precursor Ti_3AlC_2 (MAX), (b) a single-layer MXene nanosheet etched by HCl/LiF with molar ratio 1:9 on an AAO substrate.

530.8 eV can be respectively attributed to O–Ti and O–Ti/OH, the peak at 531.9–532.0 eV can be attributed to O–C/OH, and the peak at 533.1 eV can be attributed to free water molecules. Fig. 8(d) is the Ti2p of MXene. Three asymmetric double-peaks have been identified at 455.9/461.0 eV, 456.6/462.1 eV and 457.9/463.5 eV. They are respectively labeled as Ti (II), Ti (III), and Ti–O. These doublet structures are related to the MXene: Ti–C at the core of the layers with the peak at 455.0 eV, Ti (II), Ti (III), and Ti–O
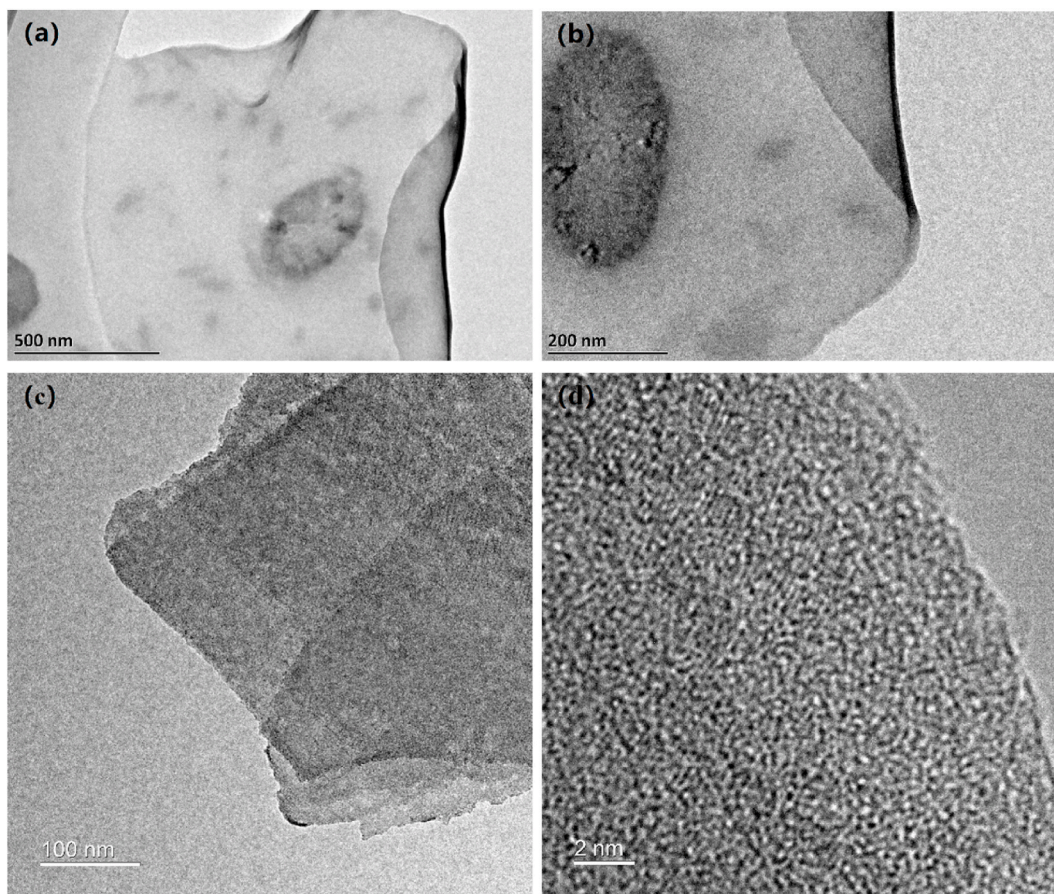
Fig. 6. TEM of sample F9 in Table 2 (a) a single-layer MXene nanosheet and (b) enlarged monolithic with smooth layer edge, HRTEM of sample F9 in Table 2 (c) two overlapping MXene nanosheets and (d) the fine structure of MXene nanosheet at a scale of 2 nm.

corresponding to Ti atoms bonded with surface functional groups and C atoms. Furthermore, the peak centered at 459.2 eV is attributed to the presence of Ti–F, which can be cross-validated by deconvolution of the F1s peak at 684.8 eV as shown in Fig. 8(e).

3.4. Thermal self-crosslinking of MXene membrane

MXene two-dimensional nanosheets were dispersed into a DI solution, and an MXene membrane was prepared using the vacuum filtration method. The MXene membrane was then subjected to thermal treatment to study the effect of the thermal self-crosslinking temperature on the structure of the MXene membrane.

The thermally treated membranes at 25 °C, 80 °C, 110 °C, 140 °C and 170 °C were named PMM, SMM-80, SMM-110, SMM-140 and SMM-170, respectively. As shown in Fig. 9(a), XRD characteristic peak of the MXene (002) shifts to a larger angle with increasing temperature. The interlayer spacing of the thermally self-crosslinked MXene membranes can be calculated in Fig. 9(b). In Fig. 9(b), the layer spacings of the MXene membranes were 0.433, 0.393, 0.386, 0.379, 0.354 nm for thermal treatment at 25 °C, 80 °C, 110 °C, 140 °C and 170 °C, respectively. It decreases steadily with increasing temperature before 140 °C. But the decrease becomes more pronounced at 170 °C. This suggests the decrease in layer spacing below 140 °C is mainly due to the removal of free water between the sheets. The thermal self-crosslinking reaction between the MXene nanosheetss occurs at temperatures of 140 °C and above.

The FTIR spectroscopy results for different thermal treatment tempreatures in Fig. 10(a) show the adsorption peak of bound water molecules (3450 cm^{-1}) and hydroxyl groups (1650 cm^{-1}) decrease with increasing temperature. Additionally, new peaks of the SMM-140 (140 °C) at 780 cm^{-1} and 870 cm^{-1} in Fig. 10(b) confirm the formation of Ti–O–Ti bonds between the nanosheets in the MXene membrane [37,38]. In Fig. 10(b), the same phenomenon occurs in the SMM-170 (170 °C) at 780 cm^{-1} and 870 cm^{-1}. However, no obvious peaks are found in the same locations of the PMM (25 °C), SMM-80 (80 °C), and SMM-110 (110 °C). It further verifies the thermal crosslinking process between the nanosheets in the MXene membrane is carried out at 140 °C.

3.5. XPS analysis and gas separation

XPS analysis of PMM and SMM-170 in Fig. 11(a) reveals that the proportions of the bonds C–Ti–O (i) and C–Ti–O (ii) changed in
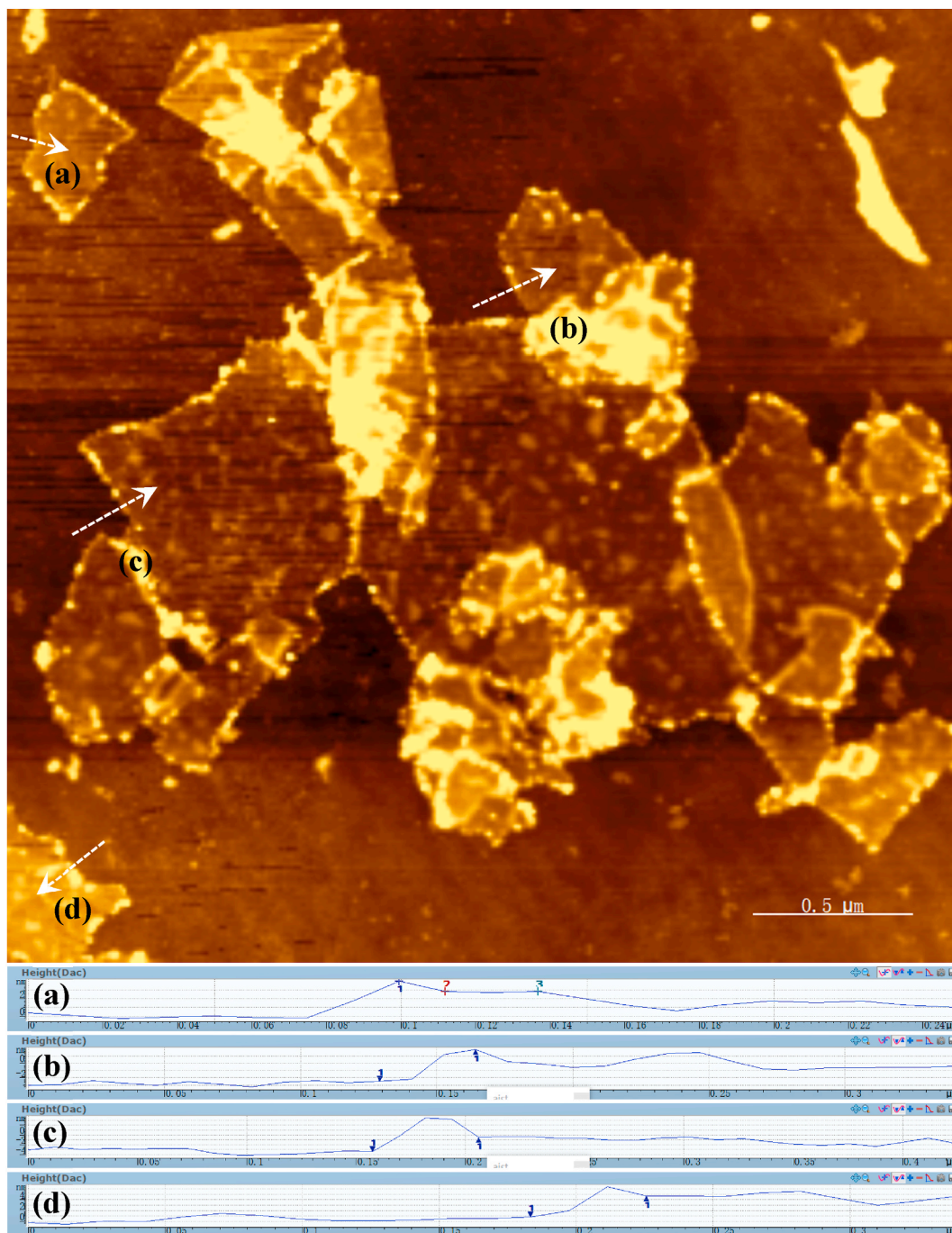
Fig. 7. AFM measurements of MXene nanosheets (sample F9 in Table 2) within a 3 μm × 3 μm scan area, where (a), (b), (c) and (d) are the thicknesses of a single MXene nanosheet measured at four dispersed locations.

both samples. In PMM, the C–Ti–O (i) and C–Ti–O (ii) are 31.97 % and 8.62 %, respectively, and the C–Ti–OH is 38.77 %. In SMM-170, the proportions of the C–Ti–O (i) and C–Ti–O (ii) increase to 43.14 % and 19.47 %, respectively, while the C–Ti–OH decreases to 14.81 %. This indicates that more Ti–O–Ti are generated between the MXene nanosheets in SMM-170, meaning that a thermal self-crosslinking reaction has occurred in the layers of the SMM-170 membrane. It also prove that the interlayer spacing of the MXene layers can be controlled by adjusting the crosslinking temperature. Additionally, the content of TiO_2 in the PMM and SMM-170 was 6.86 % and 6.79 %, respectively, indicating that the MXene is not oxidized to form TiO_2 during the thermal self-crosslinking process. Single-gas permeation experiments were performed using the SMM-170, with the transport channel of ~0.35 nm and lateral size distribution of most nanosheets 350 nm. The results are shown in Fig. 11(b). The gas permeance is mainly determined by the gas
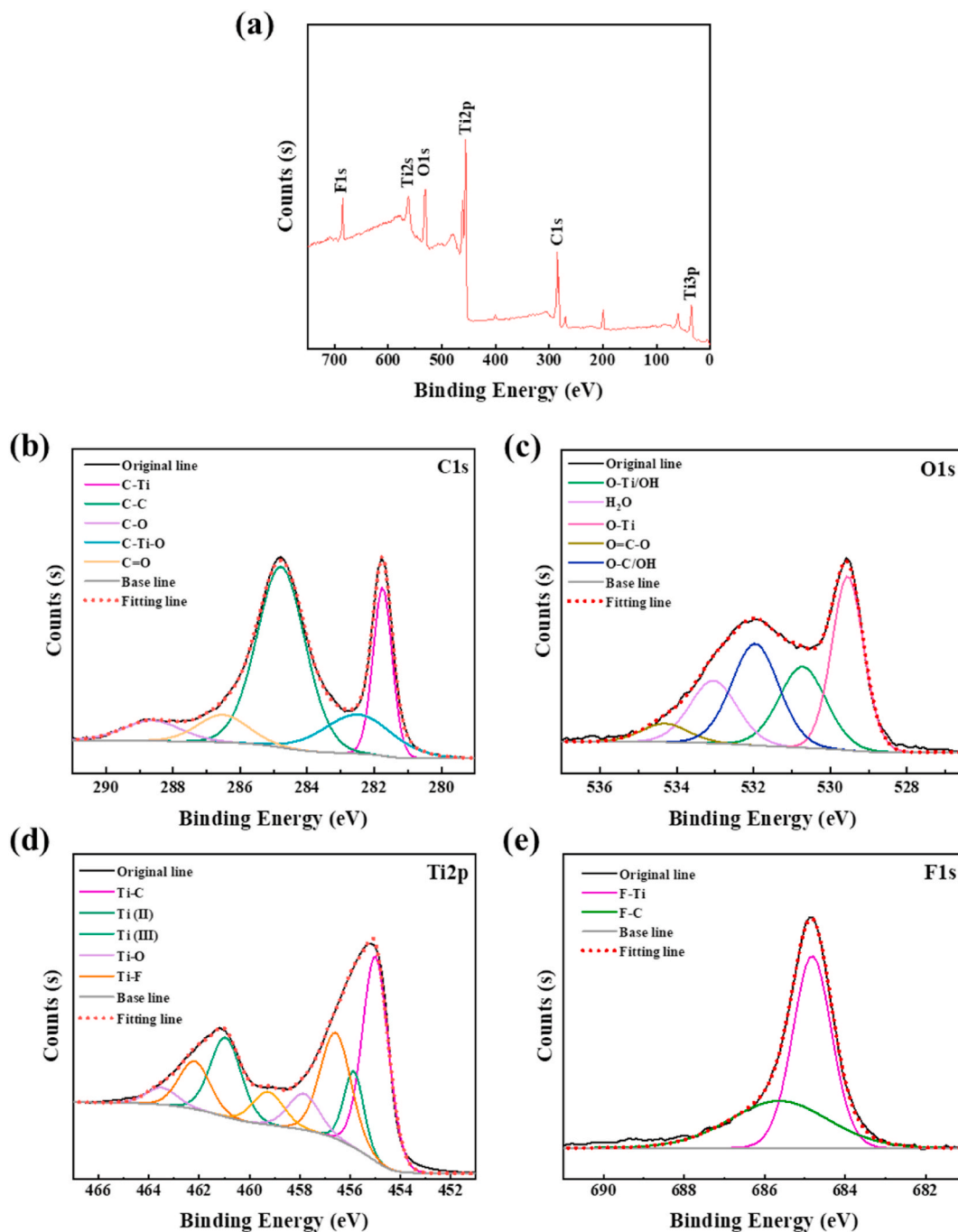
Fig. 8. XPS spectrum of MXene nanosheets (sample F9 in Table 2), High-resolution XPS spectra of (a) origin, (b) C 1s, (c) O 1s, (d) Ti 2p and (e) F 1s of MXene, respectively.

kinetic diameter rather than its molecular weight, proving a molecular sieving (size exclusion) mechanism. Moreover, by calculating the ideal selectivity (α) of H_2/CO_2, H_2/N_2, and H_2/CF_4, we believe that the α of H_2/CO_2 is very close to, the α of H_2/N_2 is equal to, and the α of H_2/CF_4 is far higher than the Knudsen coefficient. This initial evidence underscores the efficacy of the thermal regulation method in gas separation, where the selectivity of H_2/CF_4 achieves an inspiring value of 23.0.

4. Conclusions

MXene nanosheets, produced at 40 °C with etchant HCl/LiF at Al^{3+}: F^- ratio of 1:9 in solution, had single-layer structure, larger
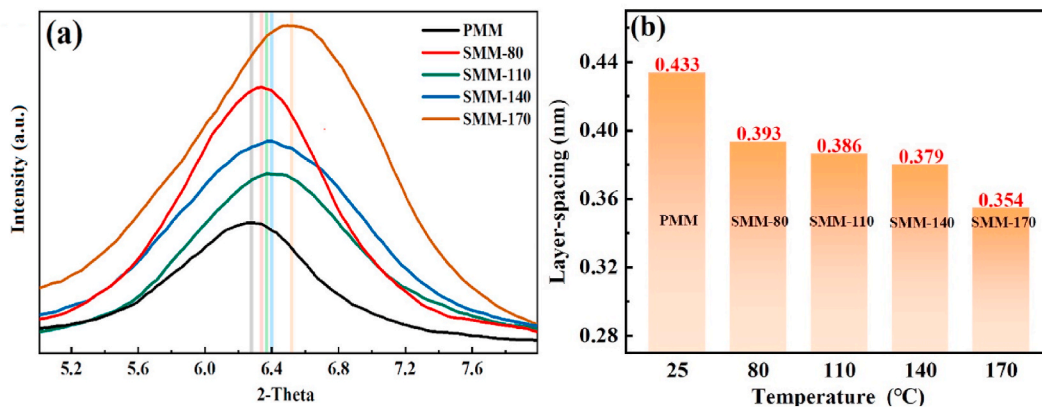
Fig. 9. (a) XRD of MXene membranes treated with different temperatures, (b) Layer spacing calculations of MXene membranes for PMM, SMM-80, SMM-110, SMM-140 and SMM-170, respectively.
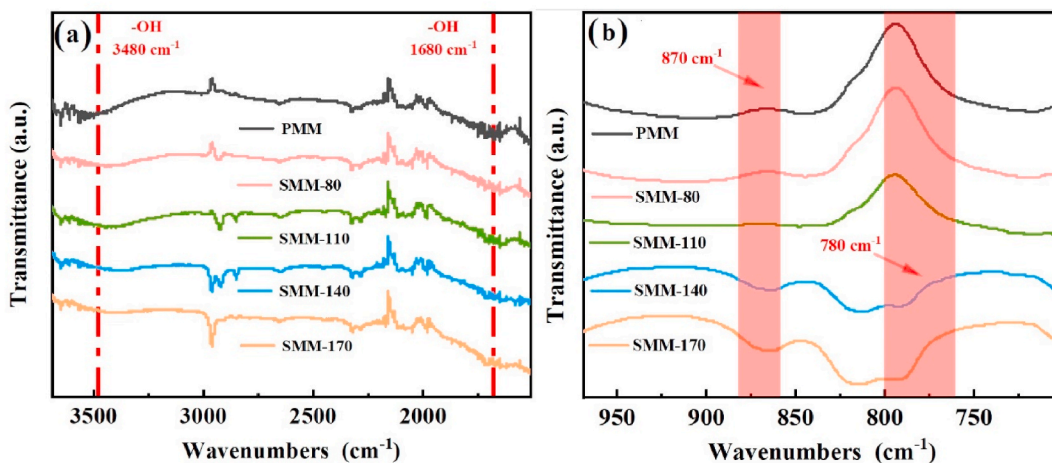

Fig. 10. FTIR wavenumbers of (a) and (b) ranging from 1510 to 3690 cm^{-1} and 700 to 970 cm^{-1} for PMM, SMM-80, SMM-110, SMM-140 and SMM-170 MXene membranes.
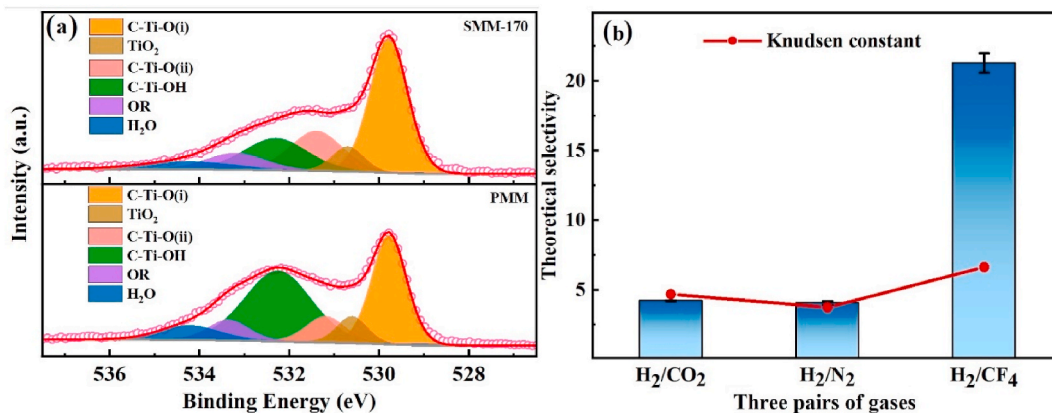

Fig. 11. Component peak fitting of XPS spectra of O1s for (a) SMM-170 and PMM MXene membranes, (b) Selective ratios: α of H$_2$/CO$_2$ close to, H$_2$/N$_2$ equal to and and H$_2$/CF$_4$ significantly higher than the Knudsen Constant.

lateral size and higher yield. The MXene obtained by the above parameters is a large single-layer 2D material, with a diameter generally larger than 500 nm, some may even exceed 1.5 μm. The thickness of the flake itself is about 2.1 nm, and the surface and edges of the flake are rich in a variety of functional groups and chemical bonds that can be adjusted for MXene membrane preparation. Self-assembly MXene membrane was prepared with vacuum-assisted filtration at room temperature. Subsequent heating allowed fine tuning of the MXene's interlayer spacing and force. At 170 °C after 30 h, thermal self-crosslinking occurred with more C–Ti–O bonds generation among the nanosheets, which endowered a more stable structure for the membrane in application. The method can demonstrate the membrane with gas molecular sieving property, with the selectivity of H_2/CF_4 as high as 23.0.

Additional information

Supplemental information for the manuscript is available online.

Data availability statement

The data generated during and analyzed during the study is not deposited into a publicly available repository, but is available from the corresponding author upon reasonable request.

CRediT authorship contribution statement

Nong Xu: Writing – original draft, Methodology, Investigation, Conceptualization. **Chen Pan:** Writing – original draft, Methodology, Investigation, Conceptualization. **Shenzhen Qu:** Validation, Investigation, Data curation. **Qiao Liu:** Writing – review & editing, Resources, Investigation. **Qing Wang:** Validation, Resources, Formal analysis. **Qiang Dong:** Supervision, Project administration, Funding acquisition. **Long Fan:** Writing – review & editing, Supervision, Funding acquisition.

Declaration of competing interest

The authors declare that they have no known competing financial interests or personal relationships that could have appeared to influence the work reported in this paper.

Acknowledgments

Appendix A. Supplementary data

Supplementary data to this article can be found online at https://doi.org/10.1016/j.heliyon.2024.e31155.

References

[1] F. Moghadam, H.B. Park, Two-dimensional materials: an emerging platform for gas separation membranes, Current Opinion in Chem. Eng. 20 (10) (2018) 28–38.
[2] G. Liu, W. Jin, N. Xu, Two-Dimensional-Material Membranes: a new family of high-performance separation membranes, Angew. Chem. Int. Ed. Engl. 55 (43) (2016) 13384–13397.
[3] P.S. Goh, A.F. Ismail, Graphene-based nanomaterial: the state-of-the-art material for cutting edge desalination technology, Desalination 356 (2015) 115–128.
[4] F. Perreault, A. Fonseca de Faria, M. Elimelech, Environmental applications of graphene-based nanomaterials, Chem. Soc. Rev. 44 (16) (2015) 5861–5896.
[5] L. Huang, M. Zhang, C. Li, et al., Graphene-based membranes for molecular separation, J. Phys. Chem. Lett. 6 (14) (2015) 2806–2815.
[6] H. Tong, Q. Liu, N. Xu, et al., Efficient pervaporation for ethanol dehydration: ultrasonic spraying preparation of Polyvinyl Alcohol (PVA)/Ti_3C_2Tx nanosheet mixed matrix membranes, Membranes 13 (2023) 430.
[7] M. Alhabeb, K. Maleski, B. Anasori, et al., Guidelines for synthesis and processing of two-dimensional Titanium Carbide (Ti3C2Tx MXene), Chem. Mater. 29 (18) (2017) 7633–7644.
[8] M. Sokol, V. Natu, S. Kota, et al., On the chemical diversity of the MAX phases, Trends in Chem. 1 (2) (2019) 210–223.
[9] M.W. Barsoum, The $M_{N+1}AX_N$ phases: a new class of solids, thermodynamically stable nanolaminates, Progress in Solid State Chem. 28 (1) (2000) 201–281.
[10] L. Verger, V. Natu, M. Carey, et al., MXenes: an introduction of their synthesis, select properties, and applications, Trends in Chem 1 (7) (2019) 656–669.
[11] Q. Liu, X. Pan, N. Xu, et al., Hypergravity field induced self-assembly of 2D MXene in polyvinyl alcohol membrane matrix and its improvement of alcohol/water pervaporation, J. Appl. Polym. Sci. 140 (16) (2023) 53740.
[12] M. Naguib, M. Kurtoglu, V. Presser, et al., Two-dimensional nanocrystals produced by exfoliation of Ti_3AlC_2, Adv. Mater. 23 (37) (2011) 4248–4253.

[13] M. Naguib, V.N. Mochalin, M.W. Barsoum, et al., 25th anniversary article: MXenes: a new family of two-dimensional materials, Adv. Mater. 26 (7) (2014) 992–1005.
[14] B. Anasori, M.R. Lukatskaya, Y. Gogotsi, 2D metal carbides and nitrides (MXenes) for energy storage, Nature Reviews Mater 2 (2) (2017) 16098.
[15] V. Natu, R. Pai, M. Sokol, et al., 2D Ti3C2Tz MXene synthesized by water-free etching of Ti3AlC2 in polar organic solvents, Chem 6 (3) (2020) 616–630.
[16] M. Ghidiu, M.R. Lukatskaya, M.Q. Zhao, et al., Conductive two-dimensional titanium carbide 'clay' with high volumetric capacitance, Nature 516 (7529) (2014) 78–81.
[17] A. Lipatov, M. Alhabeb, M.R. Lukatskaya, et al., MXene materials: effect of synthesis on quality, electronic properties and environmental stability of individual monolayer Ti3C2 MXene flakes, Adv. Electro. Mater. 2 (12) (2016) 201670068.
[18] T.S. Mathis, K. Maleski, A. Goad, et al., Modified MAX phase synthesis for environmentally stable and highly conductive Ti(3)C(2) MXene, ACS Nano 15 (4) (2021) 6420–6429.
[19] L. Ding, Y. Wei, L. Li, et al., MXene molecular sieving membranes for highly efficient gas separation, Nat. Commun. 9 (1) (2018) 155.
[20] L. Ding, Y. Wei, Y. Wang, et al., A two-dimensional lamellar membrane: MXene nanosheet stacks, Angew. Chem. Int. Ed. Engl. 56 (7) (2017) 1825–1829.
[21] J. Shen, G. Liu, Y. Ji, et al., 2D MXene nanofilms with tunable gas transport channels, Adv. Funct. Mater. 28 (31) (2018) 201801511.
[22] Y. Fan, L. Wei, X. Meng, et al., An unprecedented high-temperature-tolerance 2D laminar MXene membrane for ultrafast hydrogen sieving, J. Membr. Sci. 569 (2019) 117–123.
[23] H.E. Karahan, K. Goh, C. Zhang, et al., MXene materials for designing advanced separation membranes, Adv. Mater. 32 (2020) 1906697.
[24] J. Abraham, K.S. Vasu, C.D. Williams, et al., Tunable sieving of ions using graphene oxide membranes, Nat. Nanotech. 12 (6) (2017) 546–550.
[25] J. Wang, Z. Zhang, J. Zhu, et al., Ion sieving by a two-dimensional Ti3C2Tx alginate lamellar membrane with stable interlayer spacing, Nat. Commun. 11 (2020) 3540.
[26] C.A. Voigt, M. Ghidiu, V. Natu, M.W. Barsoum, Anion adsorption, $Ti_3C_2T_z$ MXene multilayers, and their effect on claylike swelling, J. Phys. Chem. C 122 (2018) 23172–23179.
[27] Z. Lu, Y. Wei, J. Deng, et al., Self-crosslinked MXene ($Ti_3C_2T_x$) membranes with good antiswelling property for monovalent metal ion exclusion, ACS Nano 13 (9) (2019) 10535–10544.
[28] M. Alhabeb, K. Maleski, B. Anasori, et al., Guidelines for synthesis and processing of two-dimensional titanium carbide ($Ti_3C_2T_x$ MXene), Chem. Mater. 29 (18) (2017) 7633–7644.
[29] Y. Wei, P. Zhang, R.A. Soomro, et al., Advances in the synthesis of 2D MXenes, Adv. Mater. 33 (39) (2021) e2103148.
[30] J. KimY, S.J. Kim, D. Seo, et al., Etching mechanism of monoatomic aluminum layers during MXene synthesis, Chem. Mater. 33 (16) (2021) 6346–6355.
[31] C.E. Shuck, A. Sarycheva, M. Anayee, et al., Scalable synthesis of $Ti_3C_2T_x$ MXene, Adv. Eng. Mater. 22 (3) (2020) 201901241.
[32] J. Halim, K.M. Cook, M. Naguib, et al., X-ray photoelectron spectroscopy of select multi-layered transition metal carbides (MXenes), Appli. Surface. Sci. 362 (2016) 406–417.
[33] G.M. Weng, J. Li, M. Alhabeb, et al., Layer-by-Layer assembly of cross-Functional semi-transparent MXene-carbon nanotubes composite films for next-generation electromagnetic interference shielding, Adv. Funct. Mater. 28 (44) (2018) 201803360.
[34] S.P. Surwade, S.N. Smirnov, I.V. Vlassiouk, et al., Water desalination using nanoporous single-layer graphene, Nat. Nanotech. 10 (5) (2015) 459–464.
[35] X. Wang, Q. Li, J. Zhang, et al., Novel thin-film reverse osmosis membrane with MXene $Ti_3C_2T_x$ embedded in polyamide to enhance the water flux, anti-fouling and chlorine resistance for water desalination, J. Membr. Sci. 603 (2020) 118036.
[36] X. Liu, N. Graham, W. Yu, et al., Preparation and evaluation of a high performance $Ti_3C_2T_x$-MXene membrane for drinking water treatment, J. Membr. Sci. 654 (2022) 120469.
[37] K. Qu, L. Dai, Y. Xia, et al., Self-crosslinked MXene hollow fiber membranes for H_2/CO_2 separation, J. Membr. Sci. 638 (2021) 119669.
[38] D. Li, R.B. Kaner, Graphene-based materials, Science 320 (5880) (2008) 1170–1171.